AEROSPACE REPORT NO.
TOR-2000(1550)-1

RELATIVE CALIBRATION OF THE DMSP OPERATIONAL LINESCAN SYSTEM (OLS) THERMAL FINE DATA

Prepared by

B. L. SHAW
Defense Meteorological Satellite Program
Weather and Navigation Division

January 2000

Space Systems Group
THE AEROSPACE CORPORATION
El Segundo, CA 90245-4691

Prepared for

SPACE AND MISSILE SYSTEMS CENTER
AIR FORCE MATERIEL COMMAND
2430 E. El Segundo Boulevard
Los Angeles Air Force Base, CA 90245

Contract No. F04701-93-C-0094

RELATIVE CALIBRATION OF THE DMSP OPERATIONAL LINESCAN SYSTEM (OLS) THERMAL FINE DATA

Prepared by

B. L. Shaw
Environmental Applications Center Extension
Defense Meteorological Satellite Program
Weather and Navigation Division

Approved by

J. S. Bohlson, Director
Sensor and Display Systems
Defense Meteorological Satellite Program
Weather and Navigation Division

R. J. De Lorenzo, Principal Director
Defense Meteorological Satellite Program
Weather and Navigation Division

The information in a Technical Operating Report is developed for a particular program and is not necessarily of broader technical applicability.

Abstract

The need for relative calibration accuracy across multiple Operational Linescan System (OLS) instruments for quantitative use has long been understood. Now that there are quantitative users of the fine-resolution data from the OLS, there is also a need for consistency between the smooth and fine data for a single satellite. Because the smooth format data is derived from the fine resolution imagery on the satellite, it was never anticipated there would be a significant difference (i.e., bias) between the two data streams. However, significant differences between the two data types have been identified in the thermal (infrared) channel. These differences were discovered during development of a prototype high-resolution cloud analysis system at the Air Force Weather Agency (AFWA), which uses Stored Data Fine (SDF) data as the primary input. In fact, this prototype is the first known quantitative application of the SDF-format infrared data, so it is likely that the discrepancy reported here has been present throughout the history of the Defense Meteorological Satellite Program (DMSP)/OLS program but has gone undetected. The cloud analysis prototype proved the quantitative utility of the SDF-mode data, and therefore it follows that there is a need to ensure the relative calibration accuracy between the various OLS data formats on a given spacecraft. The methodology for assessing the relative differences and development of correction coefficients is presented.

Acknowledgment

The author gratefully acknowledges those within the DMSP program who provided information and comments on the technical details of the OLS during the development of this report, including Neal Baker (Aerospace), Mike Barrett (Northrop Grumman), Ted Bland (Northrop Grumman), Roger Lieske (Northrop Grumman), and Denny Ometz (Northrop Grumman). The author is also grateful to those who reviewed this report for clarity and content, including Bruce Thomas (Aerospace).

The Air Force Weather Agency provided the DMSP data used for this study.

Contents

Figures

Tables

1. Introduction

The Operational Linescan System (OLS) is the primary instrument on the Defense Meteorological Satellite Program (DMSP) polar-orbiting satellites. Using on-board recorders, it is capable of providing visible and infrared imagery covering the entire Earth every 12 hours for centralized meteorological users. Additionally, the DMSP satellites provide direct broadcast of OLS imagery to field terminals. While the OLS has been optimized to provide imagery for use by weather forecasters in a qualitative (i.e., manual) interpretation, it has been used for many years as the primary input to an automated cloud analysis system at the Air Force Weather Agency (AFWA) known as the Real-Time Nephanalysis (RTNEPH). The RTNEPH uses the Stored Data Smooth (SDS) format data, which contains both visible and IR data at 2.5 km horizontal spatial resolution. Additionally, DMSP is often the only guaranteed source of satellite imagery available to AFWA for the Indian Ocean area, and it is often used in a semi-quantitative sense for tropical cyclone analysis.

For the current quantitative applications of OLS data, the IR channel is most critical. Accurate IR temperature information is required for the cloud/no-cloud determination, cloud height assignment, and tropical cyclone intensity estimation. Small errors in the IR brightness temperatures derived from the OLS can lead to significant cloud analysis errors (not detecting clouds where they exist or detecting clouds where there are none), especially for low clouds due to their very low temperature contrast with the surface beneath them. A few degrees of error in a cloud-top temperature derived from the IR data can mean tens of knots of error in wind speed estimation in the tropical cyclone analysis. Because SDS provides worldwide coverage and has been the only format used by quantitative applications, it has also been the format used for managing the data quality and calibration of the OLS during on-orbit operations.

In 1999, The Aerospace Corporation teamed with AFWA to develop a prototype, high-resolution, cloud analysis and forecast system (Plonski et al. 1999). This system was required to produce cloud analyses and forecasts on a 6-km grid versus the 48-km grid of the RTNEPH. The algorithms employed (Gustafson et al. 1994) require multiple pixels per grid point to perform cloud layering and typing, and the only operational satellite imagery available with the appropriate timeliness that could support this system was the fine mode data (0.5-km resolution) from the OLS. AFWA receives the Stored Data Fine (SDF) format data on a regional basis, and it can contain either the visible or IR data in the non-interleaved mode (SDFNI) or both channels in the interleaved mode (SDFI). In July 1999, this system was implemented to support Operation *Allied Force*, and marked the first known operational quantitative application of the fine-resolution OLS imagery. It was during this effort that significant differences were discovered between the IR values reported by the SDS IR data and the IR values reported by the SDF IR data from the same satellite for common scenes. Although some differences were expected due to the coarser radiometric quantization of the SDF IR data (64 steps across the dynamic range for SDF versus 256 steps for SDS), it was assumed these differences would not exhibit a significant bias. However, this was not the case. When compared to the SDS IR data (i.e., assume it is "truth"), the SDF IR values exhibited a significant cold bias on all three satellites that were providing both formats at the time (F-11, F-12, and F-13). Since the AFWA ingest system promotes the fine-mode 6-bit data into an 8-bit byte, one would expect the differences between the two to be within 4 steps on a 256-step scale. However, the bias we observed was on the order of 10 counts. This difference had a significant impact on the prototype cloud analysis system, since the

cloud detection thresholds are based on running statistics of the OLS-derived IR temperatures vs. predicted clear-scene surface temperature differences. These statistics are needed globally, so the SDS data is used to compute them. Thus, the cold bias in the SDF data caused an over-detection of low cloud when compared to thresholds computed from the SDS data.

This paper presents the work done subsequent to the discovery of the bias to quantify it for each of the available satellites. In the following section, a brief overview of the characteristics of the OLS is provided. In Section 3, the methodology of how this analysis was done is presented. In Section 4, the results of the analysis are presented along with derived calibration equations to correct for the bias. In Section 5, conclusions and recommendations are presented.

2. OLS Characteristics

The OLS is a cross-track oscillating scanner that employs a Cassegrain telescope and a series of lenses and mirrors for relay of the radiant scene energy to the three different detectors. The scanning mechanism and on-board data processing has been designed to provide nearly constant cross-track horizontal resolution, making the OLS unique in this aspect compared to other operational meteorological satellites. The OLS is described in detail in the Technical Operating Report, Block 5D-2 Operational Linescan System (Westinghouse 1981) and in the Defense Meteorological Satellite Program Block 5D-2 Compilation (The Aerospace Corporation 1986).

The T-detector is a two-segment, mercury-cadmium-telluride (HgCdTe) detector used for sampling the longwave infrared spectrum from 10.3 to 12.5 microns across a dynamic range of 190K to 310K. The high-resolution detector (HRD) is a three-segment, silicon photoconductive diode for sampling the 0.4-1.1 micron visible band under daylight conditions. The photomultiplier tube (PMT) detector is a gallium arsenides (GaAs) opaque photocathode that serves as the detector for nighttime-visible imagery. Remaining discussion will focus solely on the IR component ("T-channel") of the OLS and only with respect to the stored data formats (SDF and SDS).

The two segments of the T-detector are processed in two identical parallel paths. The analog electronics provides for amplification of the detector signals, clamps the bias offset level to a DC voltage reference, applies the commandable gain and level adjustments, and then linearizes the signal to equivalent blackbody temperature from radiance using a five-point (six linear segments) shaper function based on Planck's Law. After linear shaping, the processing of the smooth infrared (a.k.a. thermal smooth or TS) and the fine infrared (a.k.a. thermal fine or TF) data progresses along two separate paths.

For the TF path, after the data from the two segments has been passed through the shaper, they are sent through a switching gate, which selects the appropriate detector output, based on scanner angle. The left (right) detector is used for angles between 41 degrees and 56 degrees (edge of scan) to the right (left) of the nadir position. At angles less than 41 degrees from nadir, the two segments are summed and averaged. The resulting data is passed through an analog 40-kHz, 5-pole, low-pass Butterworth filter. This filter provides an analog signal output that ranges from 0.0 to 5.0 across the 190K to 310K dynamic range. For SDF data, this analog output is then sampled at the appropriate wow/flutter clock rate and passed through an analog-to-digital converter that digitizes the signal into 6-bit values (0-63 levels) and outputs 7322 samples per scan line.

For the TS path, both segments are summed and averaged across the entire scan and then passed through an 8-kHz, 5-pole, low-pass Butterworth filter. Like TF, the TS data is then corrected for wow and flutter using 1/25 of the wow/flutter clock and then passed into an analog-to-digital converter. The transform function in the TS analog-to-digital converter differs from the TF processing in that it scales the data by 80% of the dynamic range. This is to allow the sum of five pixels to be stored in a 10-bit accumulator in preparation for digital averaging of five successive scanlines. The resulting output of the scaling and A/D conversion consists of 1465 8-bit samples with values between 0 and 204. Each sample is stored into an appropriate 10-bit memory location

(1-1465) in the OLS formatter. As successive scan lines are sent in, each sample is added to the running sum of the previous sample at that location. After five scan lines have been processed, the sums are divided by four (not five, since the data was pre-scaled to 4/5 of the dynamic range) to provide a resulting 8-bit (0-255) value for each smooth sample.

In summary, the SDS data should be essentially equivalent to a five-by-five averaged version of the SDF, since it is produced by passing the fine data through an analog filter to provide the smoothing in the cross track and then averaged digitally over five successive scan lines. However, the results we have seen indicate a bias in the SDF IR values when compared to collocated SDS values from the same satellite. The next section describes the methodology we used to quantitatively compare the two different data streams.

3. Methodology

The basic steps involved in performing this study consisted of the following: data collection, SDF to SDS co-registration and re-scaling, SDF vs. SDS statistical comparisons, and derivation of SDF error correction equations. Each of these steps is described in detail below.

3.1 Data Collection

The DMSP Environmental Applications Center Extension is collocated with AFWA and has routine access to all of its conventional meteorological data and satellite data. All DMSP data ingested at AFWA is automatically transmitted via File Transfer Protocol (FTP) directly to a Sun Ultra Enterprise 4000 server located within the lab. Therefore, data collection consisted of selecting SDF and SDS data files provided from the same orbit from a given satellite. At the time the bias was noticed during the cloud analysis project, AFWA was receiving OLS imagery from four satellites: F-11, F-12, F-13, and F-14. However, F-14 was only providing SDS data due to three of the four data recorders having failed on orbit. The other three were providing both SDS and SDF, and a "cold bias" was noted in all three of these OLS instruments when inspected manually. However, subsequent to developing the tool for performing quantitative analyses on these data sets, F-11 stopped providing SDF format, so no quantitative comparisons are presented for this satellite.

The format of the data received in the lab is known as the "simple" format and provides the imagery in its original satellite viewing geometry and contains all necessary ancillary data provided by the spacecraft for Earth location, etc. For DMSP, all pixel values are saved into an 8-bit byte. In the case of SDS, visible data is provided only as a 6-bit value, with the 6 bits being stored in the 6 most significant bits of the byte. In the case of SDF, both channels are received as 6-bit values and are stored in the 6 most significant bits of the byte. Storing the 6-bit data streams in this manner results in a dynamic range of 0-252 counts in 4-step increments.

3.2 SDF to SDS Co-registration and Re-scaling

To perform rigorous quantitative comparisons between collocated data sets, a method to identically match each SDS pixel to the corresponding 25 pixels of SDF imagery was developed. In the along-track direction, this method the OLS nadir-pulse time code provided in the data stream was used to match each SDS line to five SDF lines. Per the DMSP data format specification (Westinghouse 1993), the time code provided on a smooth line of imagery is identical to the time code of the last line of the five fine-resolution scans that were integrated to produced the one smooth line. In the SDF format, the time code on a given line corresponds to the nadir time of the next successive scan. Actually, the spacecraft outputs the line just sampled with the time code of the line sampled just prior, but when this data is played back in reverse off of the recorder, the direction of the one-line offset is reversed.

Co-registration in the cross-track direction proved more challenging. The equations relating scanner angle to pixel number from Westinghouse (1981) were used to compute scanner angles for each of the 7322 SDF pixels and each of the 1465 SDS pixels. Then, the samples in the SDF having identical angles (within 1/1000 of a degree) to the SDS pixels were assumed to be the center pixels of each group of five that correspond to the SDS pixels. However, once this method was combined with the down-track co-registration method described above and the first images of count differences were displayed, it was clear that there was a slight co-registration error in the cross-track direction. Multiple tests were then run for a single case where the cross-track relationship between SDF and SDS was shifted by a varying number of pixels until the differences were minimized. It turned out that the SDF pixels needed to be shifted two samples to the right of the original expected relationship to get the best match. Therefore, the five pixels in the cross-track direction matching an SDS pixel start with the sample having an identical scanner angle and include the next four pixels to the right. This relationship was verified to be true for all of the satellites processed. Using a zero-based sample number system, the relationship between the first and last SDF pixel in the group of five corresponding to one SDS pixel can be described mathematically as:

$$SDF_{Start} = (SDS \times 5) + 2$$
$$SDF_{Stop} = SDF_{Start} + 4$$

Computationally, this would result in a problem since the last SDS pixel would need SDF pixels 7322-7326, which exceeds the maximum of sample number of 7321 (zero-based index). However, before the indexing was performed, the SDS and SDF data were trimmed for vignetting using a scanner angle threshold of +/- 55.34 degrees, so the edge of scan was never used. Additionally, all angle computations to determine segment switch points and vignetting cutoff employed the scanner-offset parameter for each satellite.

3.3 SDF vs. SDS Statistical Comparisons

The previous two steps resulted in the generation of two two-dimensional arrays: an array of SDS data with dimensions of i pixels per scan by j scans and an array of SDF data having dimensions of $5i$ by $5j$. Next, the byte values in the SDF array were re-scaled to match the scaling of the SDS array. Recall from the discussion above that the SDF data contains 6-bit values covering the dynamic range of the instrument stored left justified into an 8-bit byte, resulting in values ranging from 0-252. These values can easily be re-scaled to cover the range 0-255 using the following equation:

$$C_{new} = ROUND\left(\frac{255 C_{old}}{252}\right)$$

where C_{old} represents the value in the data file and C_{new} represents the properly scaled values ranging from 0-255.

To facilitate direct comparisons, it was desirable to build a pseudo-SDS image from the SDF data by averaging groups of 5x5 pixels in the SDF array. Once the pixel values were re-scaled, a new array of dimension (i,j) containing an average value of the 25 pixels of SDF data corresponding to each SDS pixel was created. To minimize the potential of skewing the statistics, some effort was made to

include quality control as part of the averaging process. First, any lines flagged as invalid by the ingest system were excluded from processing during computations. For each valid SDS line, all valid lines from the group of five corresponding SDF lines were used to populate a buffer, and an initial difference between each of the 25 SDF pixels and the corresponding SDS pixel was computed. Any pixels with an absolute difference exceeding 15 counts were eliminated from further processing. The remaining "good" pixels were then averaged and stored into the new decimated SDF array. At the same time the averaging was performed, statistics on the differences for that SDS point were computed and stored to another array of dimension *(i,j)* for use in subsequent processing. For each scene in the SDS array, a mean value of the corresponding valid SDF pixels was computed as well as the difference of this value and the SDS pixel. The variance of the valid SDF pixels for each SDS scene was also computed and stored in a corresponding two-dimensional array.

Once the arrays of mean difference and variance were created, these values were aggregated by detector segment (left, middle, and right). For each of these three bins, an overall cross-sample variance and mean difference was calculated. Additionally, a cross-sample variance and mean difference for all samples was computed. It should be noted that for F-12, aggregation of the statistics by segment bin was meaningless, since it has been operating in the single-segment override mode for several months.

3.4 SDF Error Correction Equation Derivation

The goal of this effort was to characterize the error in the SDF values provided by the satellite in a relative sense so that equations to correct for this error could be derived. This implies an assumption that the SDS values provide "truth." This assumption is validated by the fact that the sensor vendor uses the SDS data stream to assess and maintain the on-orbit performance of the OLS thermal channel by actively managing the gain and level settings. However, there will still be some calibration error inherent in the SDS data, so the correction applied to the SDF data results in a relative correction such that it provides results more consistent with the SDS data from the same satellite.

Although the actual results are presented in the following section, it became clear from initial scatter plots of the SDF vs. SDS differences (herein referred to as the "SDF error") that the error with respect to SDS value was somewhat linear in nature. Therefore, linear regression was chosen as the method to develop a function to correct for this error. After computing the pseudo-SDS data using the averaging process described above, the differences and SDS values were input into linear regression function to derive slope and offset values to be used in the linear correction equation. This equation was then applied to the pseudo-SDS data and differences recomputed to assess the impact of the correction. Like the statistical computations, the linear regression used only the valid points as flagged during the initial processing. The coefficients were derived for each segment bin as well as for the entire image. However, there were no noticeable differences noted by segment, so the values for the each segment are not discussed any further.

4. Results

The quantitative results corroborated our initial qualitative assessment of a cold bias in the SDF data. The characteristics of the error were similar for both satellites analyzed quantitatively (F-12 and F-13), with F-12 having a slightly more pronounced bias. Namely, the amount of cold bias varies with scene temperature, with warmer scenes exhibiting a greater cold bias in the SDF than colder scenes. Figures 1a and 1b (Appendix) contain two images constructed from the differences between the SDF and SDS data from F-13 for a cold scene and a warm scene, respectively. In these images, the darker shades (blue) indicate a cold bias and the lighter shades (yellow) represent a warm bias. The variability of the bias as a function of temperature is apparent in the non-homogeneous portions of the imagery. Cold clouds against a (relatively) warm background are apparent as shades of gray or yellow against shades of blue, because the clouds are exhibiting colder temperatures where there is less bias and are contrasted against a relatively warm background where the bias is more significant.

Figures 2a and 2b are scatter plots of the SDF-SDS difference versus the value of the SDS pixel. Again, the nature of the bias as a function of temperature is very evident by the slope of the "best fit" line generated as a result of the linear regression as described above. Similar scatter plots were generated for each detector segment individually (left, right, and "middle") and the results were similar and therefore are not shown. Figures 2 and 3 contain images and plots for two F-12 cases analogous to the F-13 cases shown in Figures 1 and 2.

Tables 1 and 2 report the results from the analysis of eight F-12 cases and nine F-13 cases. For each case, mean scene values from the SDS and SDF data and their differences are summarized. Additionally, the coefficients computed from linear regression of the SDF-SDS difference vs. SDS value are shown.

From the table values, the average differences on F-12 are on the order of twice the amount observed on F-13. However, the behavior of the error term as a function of scene is similar for both satellites.

The average slope and offset values for each satellite can be used to correct the SDF values via the following equations:

$$E_{SDF} = mC_{new} + b$$
$$C_{Corr} = C_{new} - E_{SDF}$$

where E_{SDF} is the predicted SDF-SDS error (in 8-bit counts), m is the slope value, b is the offset value, C_{new} is the raw SDF count re-scaled to an 8-bit byte, and C_{Corr} is the corrected 8-bit SDF count value.

These equations were applied to additional F-12 and F-13 cases to determine the improvement gained. Figure 5 shows scatter plots generated from comparing the corrected SDF data to the coincident smooth data using the same algorithm described above. Clearly, the majority of the bias is removed. The remaining differences appear to be random and are simply the result of the SDF

data having reduced quantization and additional "noise" to gain the benefit of improved horizontal spatial resolution.

Table 1. Mean Values for F-12 Cases and the Resulting Regression Coefficients

Mean SDS Value	Mean SDF Value	Difference	Cal. Slope	Cal. Offset
162.9	157.3	-5.6	-0.0335	-0.06
168.6	162.0	-6.6	-0.0397	0.72
224.8	216.7	-8.1	-0.0377	0.69
184.4	177.7	-6.7	-0.0364	0.26
181.5	174.9	-6.6	-0.0397	0.85
226.1	217.6	-8.5	-0.0330	-0.34
182.9	176.2	-6.7	-0.0364	0.22
190.0	182.7	-7.3	-0.0416	1.03
Mean Values		-7.0	-0.373	0.42

Table 2. Mean Values for F-13 Cases and the Resulting Regression Coefficients

Mean SDS Value	Mean SDF Value	Difference	Cal. Slope	Cal. Offset
138.6	134.8	-3.8	-0.0215	-0.65
171.0	166.7	-4.3	-0.0333	1.22
145.9	142.5	-3.4	-0.0258	0.04
194.0	189.0	-5.0	-0.0266	0.31
170.4	166.3	-4.1	-0.0281	0.51
136.1	133.0	-3.1	-0.0161	-1.26
186.1	181.6	-4.5	-0.0255	0.00
170.1	165.9	-4.2	-0.0286	0.50
169.0	164.9	-4.1	-0.0271	0.36
Mean Values		-4.1	-0.0258	0.11

5. Conclusions and Recommendations

Quantitative analysis has shown a repeatable and consistent cold bias in the IR channel of the OLS SDF data that increases as a function of scene temperature when compared to the corresponding SDS data. For quantitative applications that rely on thermal fine data in the future, it will be important to correct for this bias. An analysis of on-board data processing indicates this bias is likely introduced by differences in the filters used for SDF and SDS and/or the differences in the A/D converters employed. It would be interesting and useful for the OLS vendor to modify their prelaunch calibration and test procedures to try and isolate where these differences are introduced, which could ultimately lead to OLS hardware and/or software modifications to ensure cross-calibration between the two data types.

Alternatively, this paper has demonstrated that the bias can be removed using a linear calibration correction equation. Replacement tables to perform the correction for each satellite could be generated by intercomparing several sets of SDS and SDF data using the method described above to generate the necessary coefficients. This solution would have no impact on the flight hardware or software, but would require that all users of SDF data desiring accurate cross-calibration be modified to use these coefficients or replacement tables.

References

1. The Aerospace Corporation, 1986: *Defense Meteorological Satellite Program Block 5D-2 Compilation*. The Aerospace Corporation TOR-0086(6478-40)-1, 251 pp.

2. Gustafson, G.B., et. al., 1994: *Support of Environmental Requirements for Cloud Analysis and Archive (SERCAA): Algorithm Descriptions*. TR-94-2114, Phillips Laboratory, Hanscom AFB, MA, ADA 283240.

3. Plonski, M.P., G.B. Gustafson, B.L. Shaw, B.H. Thomas, and M. Wonsick, 1999: "High Resolution Cloud Analysis and Forecast System," Preprints, *10th Conference on Satellite Meteorology and Oceanography*, Long Beach, CA, Amer. Meteor. Soc., [in press].

4. Westinghouse Defense and Electronics Systems Center, 1981: Technical Operating Report, Block 5D-2 Operational Linescan System. Westinghouse Document #81-0267, Baltimore, MD, 409 pp.

5. Westinghouse Electric Corporation, 1993: *DMSP Data Specifications*, IS-YD-821, Revision C. Westinghouse Electric Corporation, Electronic Systems Group, Baltimore, MD, 64 pp.

APPENDIX

Figure 1a. Image of differences between SDF and SDS for a relatively cold F-13 scene.

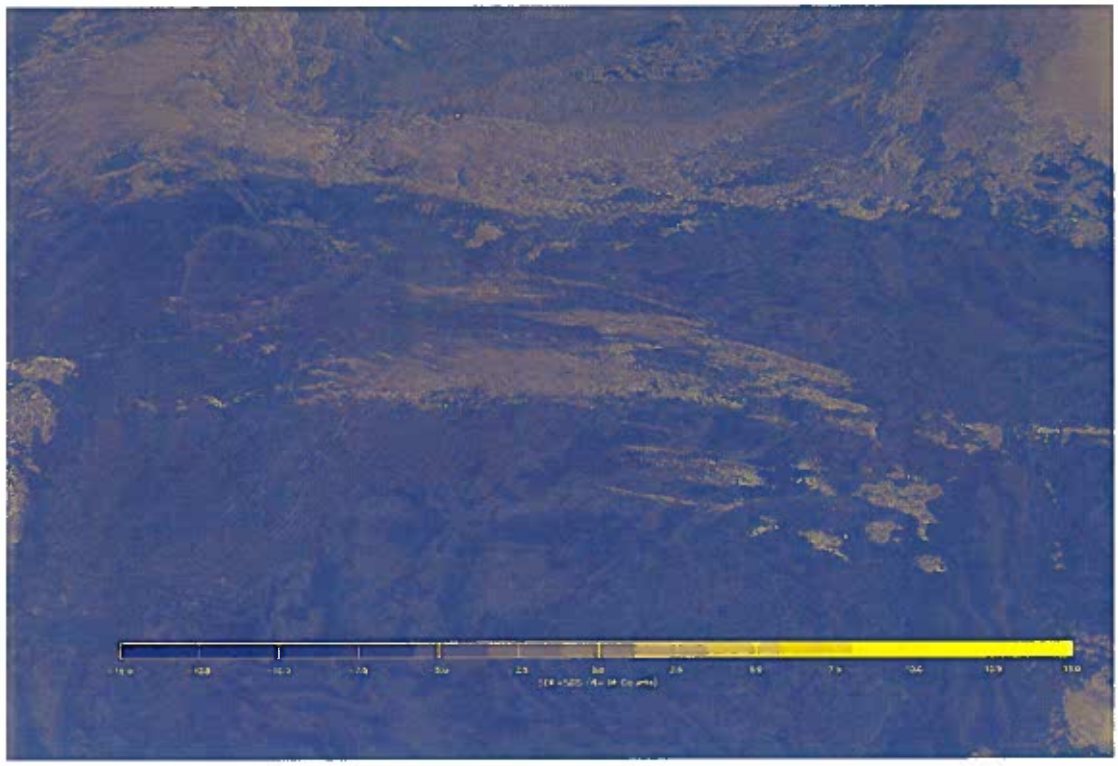

Figure 1b. Image of SDF-SDS difference for a relatively warm F-13 scene.

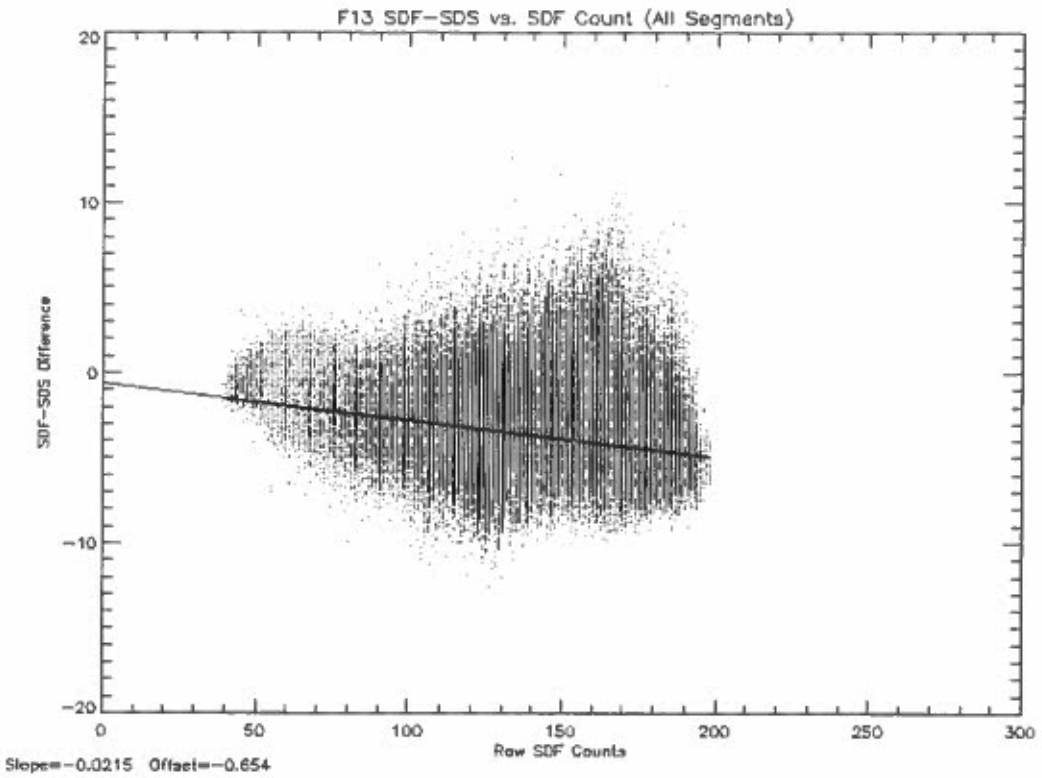

Figure 2a. Scatter plot of SDF-SDS difference vs. SDS value for F-13 cold scene.

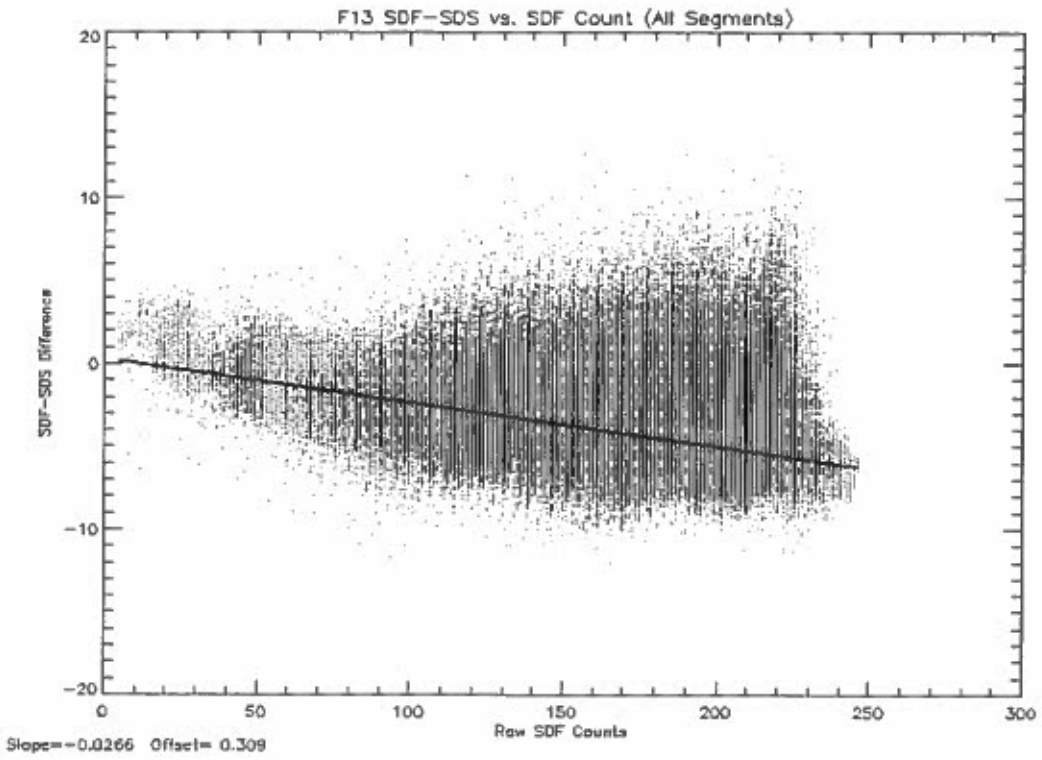

Figure 2b. Scatter plot of SDF-SDS difference vs. SDS value for F-13 warm scene.

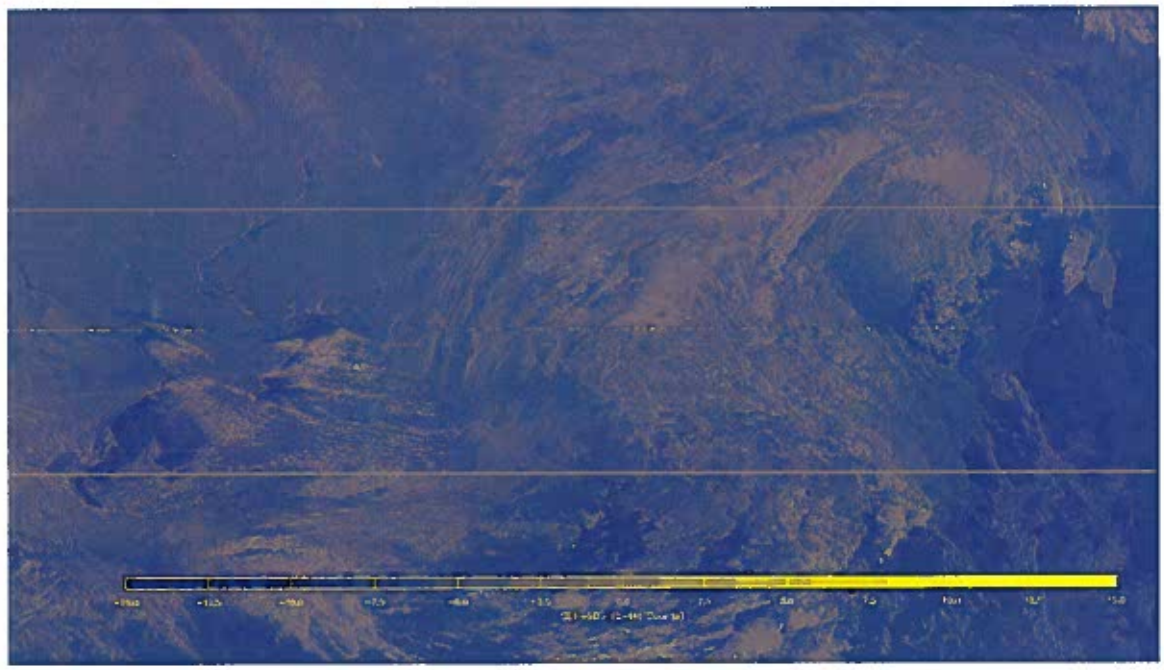

Figure 3a. SDF-SDS difference for F-12 cold scene.

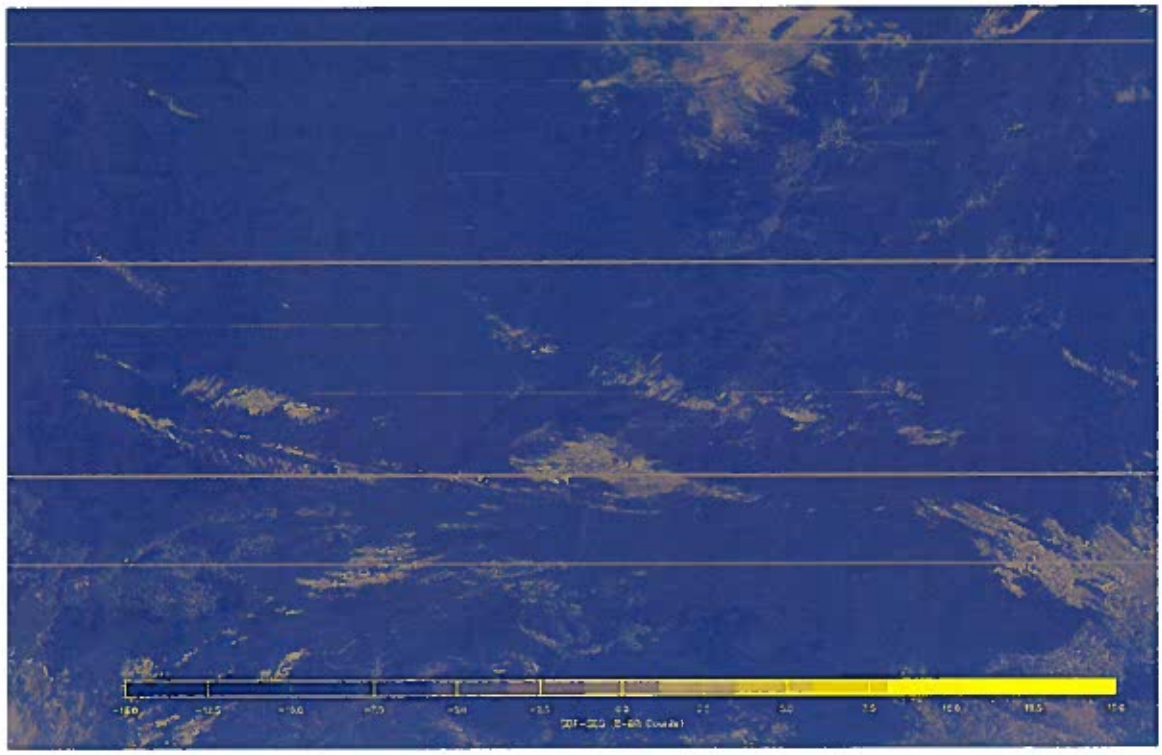

Figure 3b. SDF-SDS difference for F-12 warm scene.

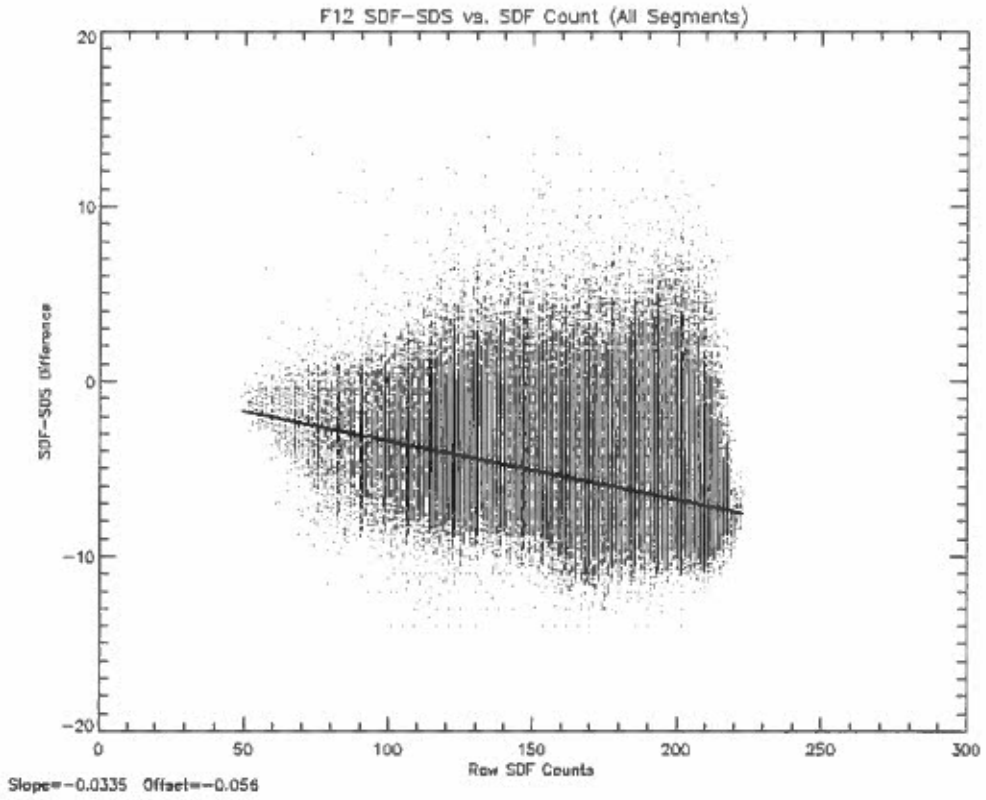

Figure 4a. SDF-SDS difference vs. SDS value for F-12 cold scene.

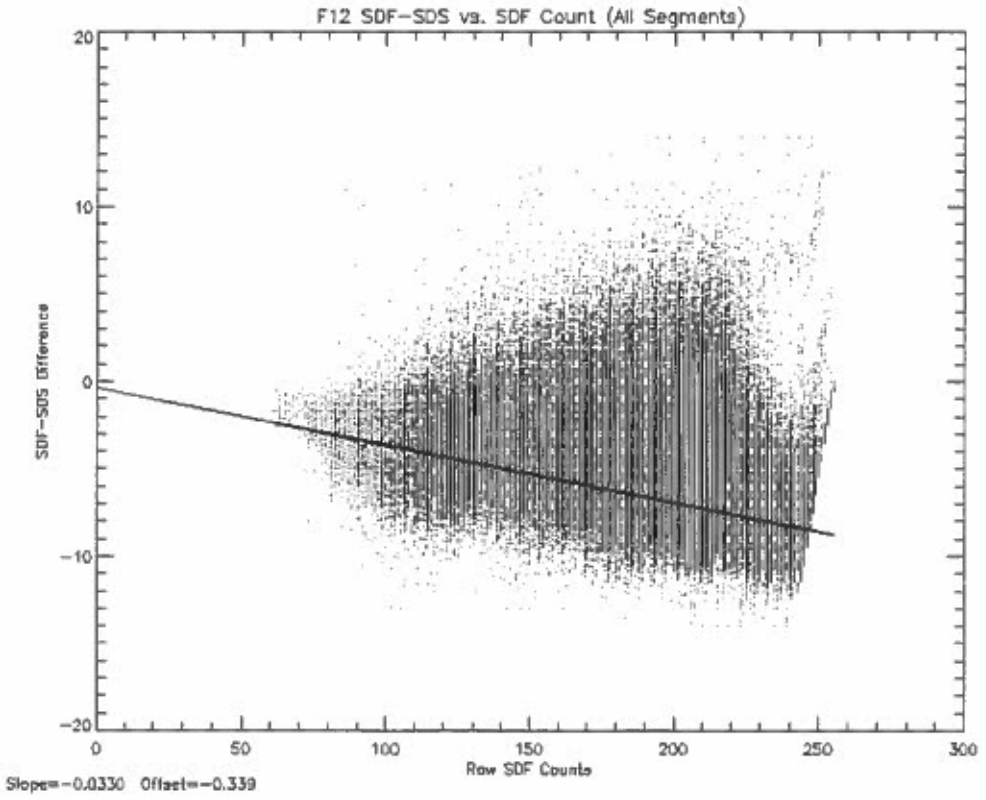

Figure 4b. SDF-SDS difference vs. SDS value for F-12 warm scene.

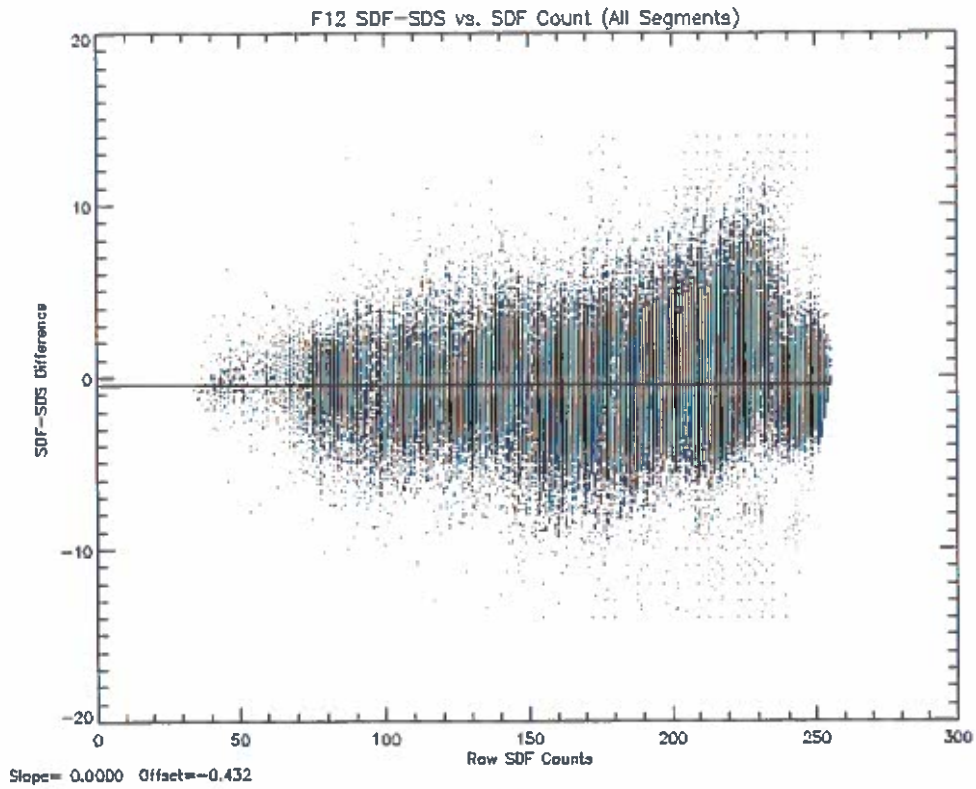

Figure 5a. Corrected SDF-SDS difference vs. SDS value for F-12.

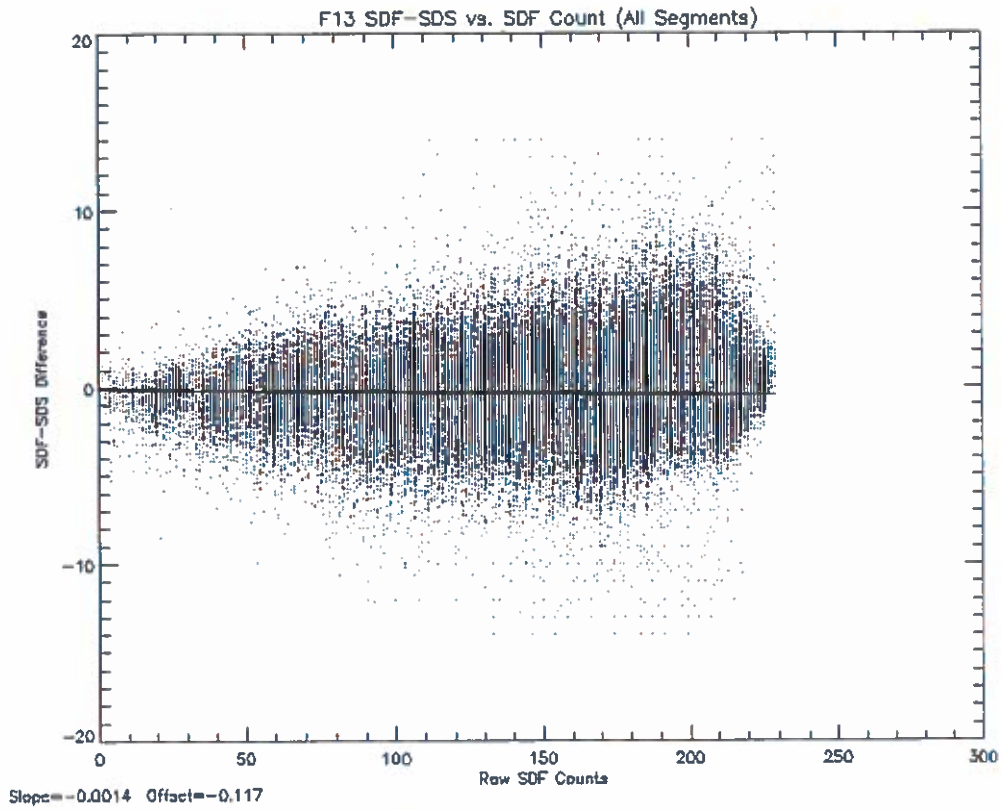

Figure 5b. Corrected SDF-SDS difference vs. SDS value for F-13.